Journal of Computer Assisted Tomography
24(6):958–964

Quantification and Minimization of Magnetic Susceptibility Artifacts on GRE Images

John D. Port and Martin G. Pomper

Purpose: The purpose of this work was to determine the optimal imaging parameters for minimization of metallic susceptibility artifacts during gradient echo (GRE) imaging.

Method: We performed GRE imaging of titanium screws in a nickel-doped agarose gel phantom, systematically varying several parameters to characterize and quantify susceptibility artifacts.

Results: The greatest reduction in artifact size came from using a short TE; increasing the frequency matrix and decreasing the slice thickness also contributed substantially to reducing the artifact size. Whenever possible, implanted prostheses should be aligned with the main magnetic field to minimize artifact size. Parameters with negligible effect on artifact size included bandwidth, phase encode matrix, and field of view.

Conclusion: Radiologists can easily adjust the above parameters in their imaging protocols to improve GRE image quality in patients with implanted metallic devices.

Index Terms: Magnetic resonance imaging—Magnetic resonance imaging, physics and instrumentation.

Metallic susceptibility artifacts from implanted medical devices often obscure regions of interest, leading to indeterminate or incorrect interpretations. It is well known that such artifacts are more pronounced using gradient echo (GRE) techniques than spin echo (SE) techniques (1,2). Whereas several studies have empirically examined optimizing various imaging parameters to minimize susceptibility artifacts using the SE technique (2,3–6), little work has been done for the GRE technique (1). We imaged titanium screws in a nickel-doped agarose gel phantom, systematically varying several GRE imaging parameters to characterize and quantify susceptibility artifacts.

METHODS

A standard, widely used orthopedic titanium bone screw measuring 28 × 2.7 mm (Synthes; Monument Colorado; total volume 0.181 ml) was suspended in an agarose gel phantom formulated to simulate the T1 and T2 characteristics of gray matter (7). Images were obtained using a GE Signa 1.5 T MR scanner. Sequences included an SPGR (spoiled GRE) sequence, a standard SE sequence, and a traditional GRE sequence. A "standard slice" was defined with the screw placed with its long axis perpendicular to the main magnetic field (B_0) and with frequency matrix of 256 pixels, phase matrix of 256 pixels, field of view (FOV) of 80 mm, slice thickness of 6 mm, one excitation, and the frequency direction (i.e., readout gradient) parallel to B_0. The readout gradient direction was parallel to B_0 for all experiments and, as such, perpendicular to the screw axis in all experiments except for the angle to B_0 experiment in which the screw axis was systematically varied. Sequence-specific parameters were as follows: for SPGR sequences, TR 35 ms, TE 5 ms, flip angle 45°; for SE sequences, TR 500 ms, TE 14 ms; for GRE sequences, TR 25 ms, TE minimum, flip angle 30°. Images were transferred to a PC and analyzed using Scion Image (Scion Corp., Frederick, MD, U.S.A.) by auto-thresholding the image, converting it into binary, and then counting the number of pixels in the artifact. For the few images with a poor signal-to-noise ratio (i.e., those with large matrices), the artifacts were manually traced to exclude as much image noise as possible.

RESULTS

Figure 1 shows the typical configuration of the artifact in both the coronal and the sagittal planes generated us-

From the Division of Neuroradiology, Russell H. Morgan Department of Radiology, Johns Hopkins Hospital, Baltimore, MD, U.S.A. Address correspondence and reprint requests to Dr. Martin G. Pomper at Division of Neuroradiology, Russell H. Morgan Department of Radiology, Johns Hopkins Hospital, 600 N. Wolfe St., Baltimore, MD 21287, U.S.A. E-mail: jport@welch.jhu.edu

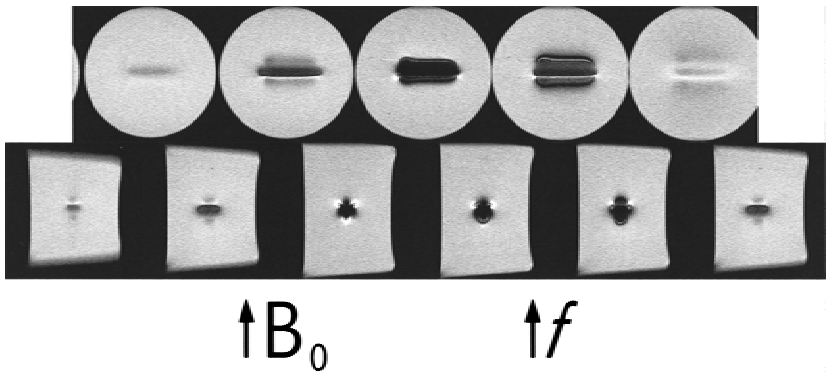

FIG. 1. Representative coronal (upper row) and sagittal (lower row) images through the screw phantom using the "standard" SPGR sequence. The axes of the main magnetic field B_0 and the frequency (readout gradient) direction *f* are indicated beneath the images in this figure as well as Figs. 2 and 4. A complex multilobed artifact is seen, with finely detailed alternating areas of signal dropout and signal hyperintensity (coronal images). The contour of the artifact depends on the region sampled. For example, in the middle of the screw (third sagittal image from the left), a six-lobed mixed signal artifact is seen, whereas at the end of the screw (rightmost sagittal image), a four-lobed hypointense artifact is seen.

ing the "standard" SPGR sequence. Note the complex halo effect with alternating areas of signal dropout intermixed with areas of increased signal. The sagittal plane demonstrates a six-lobed artifact in the center of the screw and a four-lobed artifact at the ends of the screw.

While all other SPGR parameters were kept constant, TE was varied; a dramatic increase in the size of the artifact was seen with relatively small changes in TE. Figure 2 demonstrates the imaging effects of changing TE, and Fig. 3 shows the quantitative analysis of TE on artifact size. Artifact size and TE were highly correlated ($r = 0.997$).

Bandwidth was also varied from 10.42 to 15.63 kHz, with all other parameters constant. A slight but measurable reduction in artifact size was noted with the higher bandwidths (magnitude ≈0.75%). Although the reduction in artifact size was small, artifact size and bandwidth were also highly correlated ($r = -0.968$).

The angle of the screw in relationship to B_0 was also varied, with imaging results shown in Fig. 4 and quantitative analysis in Fig. 5. Note that not only the size but the characteristics of the artifact change depend on the angle relative to B_0. When the screw is aligned with the main field, the artifact is minimal; even the threads become visible. Focal areas of increased artifact are noted only at the ends of the screw. However, as the screw reaches an angle perpendicular to B_0, the artifact completely overshadows the thread detail. A similar effect happens when using the SE sequence, but to a much lesser extent. There were minimal differences in the appearance of the artifact between the SPGR and GRE sequences. Figure 5 demonstrates the magnitude of the effect for all three sequences. Artifact size and angle to B_0 were highly correlated for the SPGR and GRE sequences ($r = 0.981$ and $r = 0.986$, respectively) but less well correlated for the SE sequence ($r = 0.750$).

As voxel volume has been linked to artifact size (2,6), we systematically varied the four parameters that determine voxel volume for a total of 16 possible combinations: frequency matrix 256 or 512 pixels, phase encode matrix 128 or 256 pixels, FOV 80 or 160 mm, and slice thickness 3 or 6 mm. Varying these parameters generated six different voxel volumes (0.146, 0.293, 0.586, 1.172, 2.344, and 4.688 mm^3); thus, there was considerable overlap of different parameters generating the same voxel volume. Figure 6 shows that there was large variability between artifact sizes depending on the different parameters used to generate a given voxel volume; correlation of artifact size with voxel volume was fair ($r = 0.445$).

The effects of individual parameters were examined. Figure 7 shows the effects of varying one parameter while keeping the others constant; the eight pairs of bars in each graph represent the eight possible combinations of the remaining parameters. Increasing the frequency matrix (Fig. 7A) had the greatest effect on the artifact size, reducing it on average by 77%. Increasing the slice thickness (Fig. 7B) also affected the artifact size, increasing it on average by 40%. Increasing the phase matrix (Fig. 7C) and the FOV (Fig. 7D) had essentially no effect on the artifact size (2% increase and 4% decrease, respectively). Correlation coefficients were excellent for artifact size and frequency matrix ($r = -0.956$), fair for slice thickness ($r = 0.248$), and negligible for phase

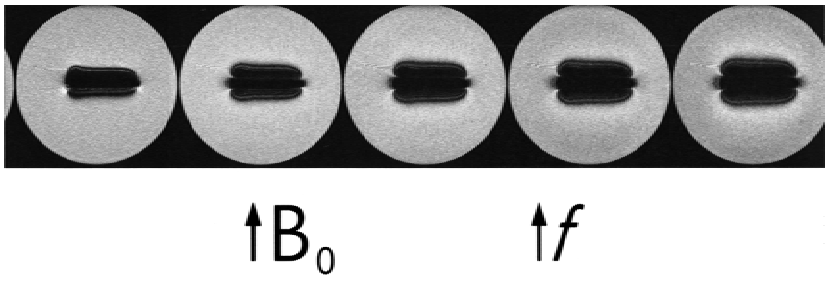

FIG. 2. Images show the effects of varying TE on artifact size. TE was increased from 5 ms (leftmost image) to 25 ms (rightmost image) in increments of 5 ms. Note a dramatic increase in artifact size with relatively small changes in TE.

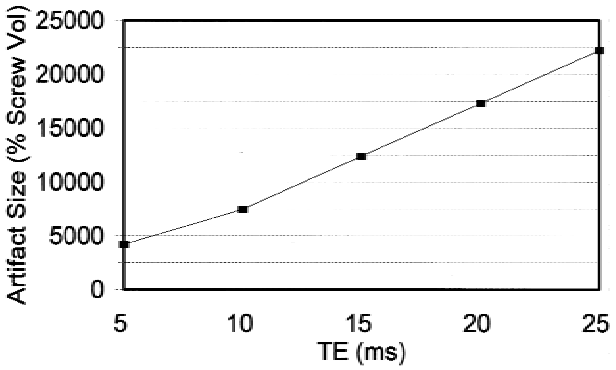

FIG. 3. Graph demonstrates the quantitative relationship between artifact size and TE. Note that artifact size is quite large compared with the actual screw size; the smallest artifact size was still 50 times larger than the actual screw volume. Furthermore, artifact size increased linearly with increasing TE; the two were highly correlated ($r = 0.997$).

matrix and FOV ($r = 0.009$ and $r = -0.002$, respectively). The ratio of FOV to frequency matrix correlated fairly well ($r = 0.665$); however, the ratio of slice thickness to frequency matrix was a better index of artifact size in our data ($r = 0.862$).

DISCUSSION

Several studies have empirically examined optimizing various imaging parameters to minimize susceptibility artifacts using the SE technique (2,3–6). These studies varied only one or two parameters at a time, and only one study examined the effects of varying parameters in GRE sequences (1). For our discussion, we will first present the most recent theory of susceptibility artifacts and then discuss our findings in the context of this theory and these previous works.

Theory of the Susceptibility Artifact

Magnetic susceptibility is a measure of the extent a substance is magnetized when placed into an external magnetic field. The magnetic field induced in the substance alters the external magnetic field, either by strengthening the field by pulling the external field lines into the substance (paramagnetic) or by weakening the field by deflecting the external field lines away from the substance (diamagnetic). All substances placed in an external magnetic field affect the field lines because of this effect; the amount of the effect is determined by the volume magnetic susceptibility of the substance.

Within a given substance or between substances with similar magnetic susceptibilities, the effects of magnetic susceptibility are similar, and the distortion of B_0 is minimal. However, at interfaces between substances with large differences in magnetic susceptibilities (e.g., air/bone or metal/tissue), the substance with the higher volume magnetic susceptibility affects the magnetic field in the substance with the lower volume magnetic susceptibility; the actual magnetic field becomes heterogeneous, resulting in geometric distortion of images as image generation requires a homogeneous magnetic field. The induced magnetic field is proportional to the strength of the external magnetic field; thus, the magnetic field distortions and subsequent image distortion are greater for high field magnets. If the substance is not moving (e.g., an implanted prosthesis), then that substance is said to induce a static magnetic field defect, which can be corrected with SE imaging.

Susceptibility artifact seen on MR images consists of three components. The first component results from signal void from the object itself; as ^{48}Ti has no nuclear magnetic moment, no signal is generated by the material itself.

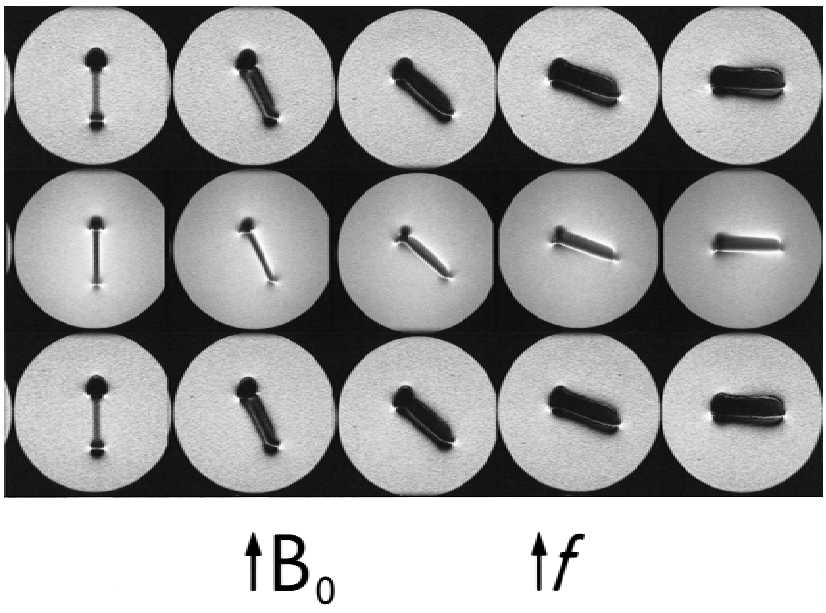

FIG. 4. Images shows the effects of varying the angle to B_0 and the imaging sequence. The three sequences used were SPGR (upper row), SE (middle row), and GRE (lower row) with the exact parameters specified in Methods. The screw was aligned with B_0 in the leftmost images (0°) and rotated to 22.5, 45, 67.5, and 90° (rightmost images) off-axis from B_0. Note how the artifact changes dramatically in size and character depending on the angle of rotation from B_0. When the screw is parallel to B_0, the artifact is minimized and fine details such as the screw's threads are visible. When the screw is perpendicular to B_0, the artifact dominates and fine details are lost. As one can see, SE imaging has much smaller artifact because of the rephasing 180° RF pulse.

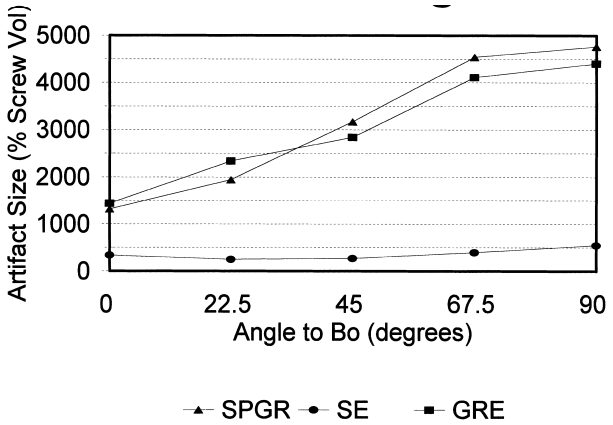

FIG. 5. Graph demonstrates the quantitative relationship between artifact size and the angle to B_0 for each of the three imaging sequences. There was little difference between the SPGR and GRE sequences, as expected, as both are GRE sequences. Artifact size increased with increasing angle to B_0 for all sequences; however, the effect was more dramatic for the GRE sequences.

The second component is due to the static magnetic field defect induced by the object. Alterations in the local magnetic field cause protons in the object and adjacent tissues to precess at a different frequency than would be expected if the object were not there (Larmour equation). As such, when a Fourier transform is performed in the frequency direction (part of the 2D Fourier transform used to reconstruct images), these altered frequencies are spatially mismapped (misregistered) onto the wrong portion of the image. If the frequency shift induced by the magnetic field heterogeneity is small, the shift is small; if it is large, the shift is large and may be beyond the range of the Fourier transform such that the signal from the tissues surrounding the object is lost. Such shifts occur only in the frequency direction and are often seen as a signal void with an adjacent high signal rim (the mismapped signal). SE imaging uses the 180° pulse to refocus the spins, thereby minimizing the effects of the local field distortion. GRE imaging does not have this pulse, so the image distortion is worse.

The third component results from the rapid falloff of the magnetic field distortion within a very small distance from the object. If such spatial variations are present within individual voxels, the phase of spins on one side of a voxel will be different from the phase of spins on the opposite side, resulting in phase dispersion within the voxel; furthermore, the phase dispersion will increase over time as spins on opposite sides of a voxel become more out of phase. This effect results in loss of signal intensity within a voxel, effectively creating a signal void near the object. Intravoxel phase dispersion is more pronounced closer to the object (where the magnetic field is more heterogeneous); it is also more pronounced the longer one waits to generate the echo. Phase dispersion is irreversible; that is, it cannot be corrected with the SE technique.

Selection of Optimal Imaging Parameters to Reduce Susceptibility Artifacts

Based on the above theory, one can essentially predict the effect of changing various MR parameters on image quality. The following paragraphs discuss how the most common MR parameters can be optimized to minimize susceptibility artifacts; our data and the current literature are discussed for each parameter.

Imaging Sequence

Susceptibility artifacts are minimized by using the SE technique (2–6,8–10). The 180° RF pulse in the SE sequence refocuses spins, thereby reversing the effects of static magnetic field defects. We also found this to be true (Figs. 4 and 5), with artifact size reduced approximately two to five times if the SE technique is used. Clearly, the SE technique is preferred when imaging patients with metallic implants. However, many times, GRE techniques are required to obtain the necessary information, especially for flow-related (phase contrast or time-of-flight) studies, volume acquisitions, and studies in which rapid imaging is needed to reduce object motion

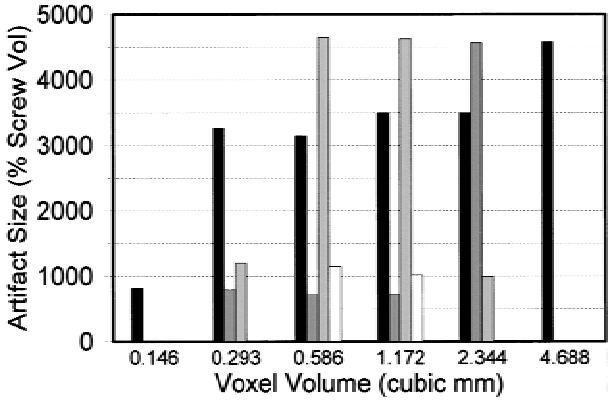

FIG. 6. Graph demonstrates the quantitative relationship between artifact size and voxel volume. The four parameters that determine voxel volume (F, frequency matrix; p, phase matrix; V, FOV; S, slice thickness) were systematically varied to yield six possible voxel volumes. Each bar in the graph represents the artifact size resulting from a single combination of parameters generating that particular voxel volume; several voxel volumes have more than one bar because different combinations of imaging parameters would generate the same volume. We found a large variation in artifact size for a given voxel; therefore, voxel volume by itself was not a good predictor of artifact size. Parameters for each voxel volume, from left to right: **0.146 mm^3:** F = 512, p = 256, V = 80, S = 3. **0.293 mm^3:** F = 256, p = 256, V = 80, S = 3; F = 512, p = 128, V = 80, S = 3; F = 512, p = 256, V = 80, S = 6. **0.586 mm^3:** F = 256, p = 128, V = 80, S = 3; F = 512, p = 256, V = 160, S = 3; F = 256, p = 256, V = 80, S = 6; F = 512, p = 128, V = 80, S = 6. **1.172 mm^3:** F = 256, p = 256, V = 160, S = 3; F = 512, p = 128, V = 160, S = 3; F = 256, p = 128, V = 80, S = 6; F = 512, p = 256, V = 160, S = 6. **2.344 mm^3:** F = 256, p = 128, V = 160, S = 3; F = 256, p = 256, V = 160, S = 6; F = 512, p = 128, V = 160, S = 6. **4.688 mm^3:** F = 256, p = 128, V = 160, S = 6.

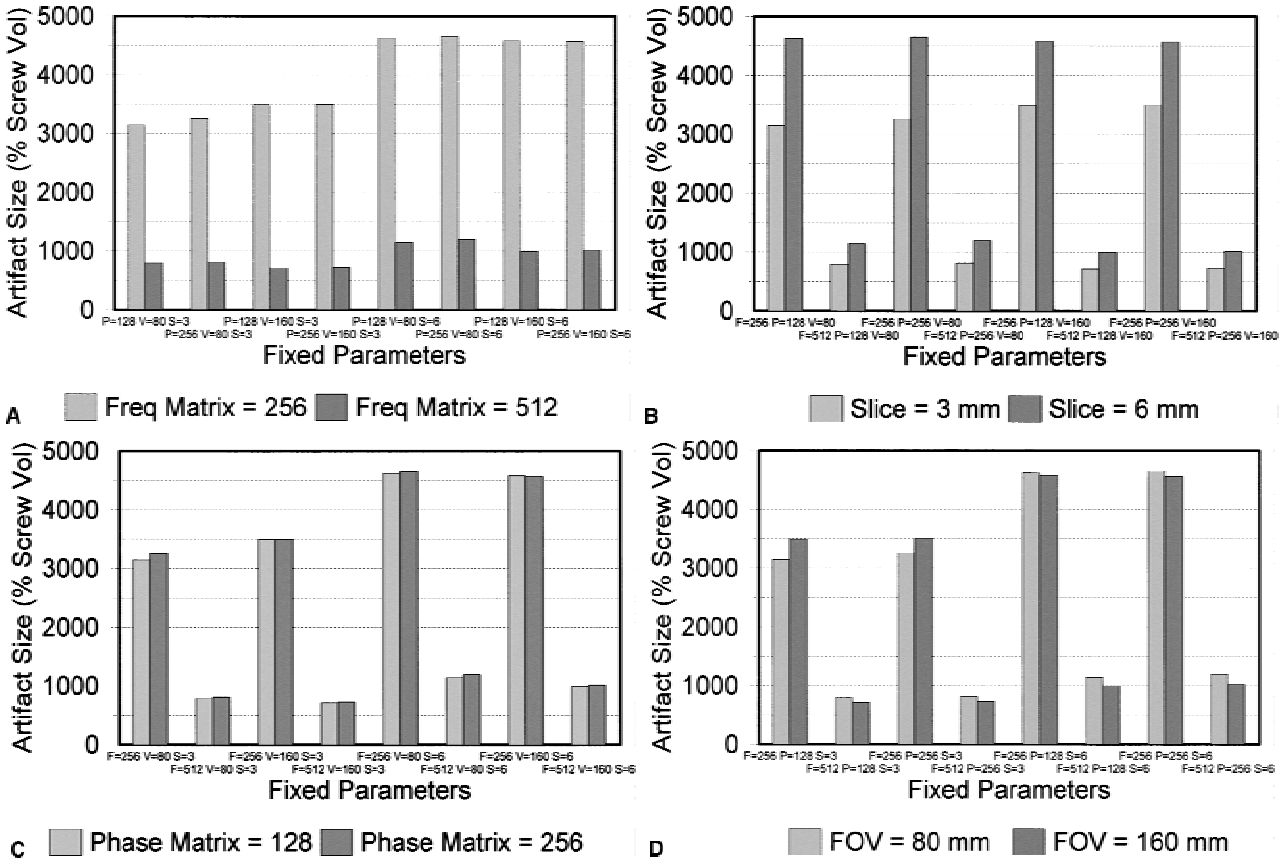

FIG. 7. Graphs demonstrate the quantitative relationships between artifact size and the individual parameters that determine voxel volume. There was a substantial reduction in artifact size when a larger frequency matrix (**A**) and a smaller slice thickness (**B**) were used. Changing the phase matrix (**C**) and the FOV (**D**) had no effect on artifact size.

(i.e., cardiac imaging). In those cases, the other parameter optimizations discussed herein can be used.

Echo Time

Susceptibility artifacts are minimized by using shorter TE (2,11,12). This occurs because there is less time for intravoxel phase dispersion to occur before the echo is regenerated. We found this parameter to have the most dramatic effect on susceptibility artifact size (Figs. 2 and 3), reducing it approximately five times when the TE was shortened from 25 to 5 ms. In clinical practice, using a shorter TE will alter tissue contrast within an image (we used phantoms where image contrast was implicitly high). However, the shortest TE that gives "acceptable" image contrast should be used.

Angle to B_0

Artifacts are minimized when the axis of object is parallel to B_0 (9,10). This occurs because the local magnetic field around the screw is distorted much less when the screw is aligned parallel to B_0 than when it is aligned perpendicular to B_0; that is, the static magnetic field defect induced by the object (and therefore the spatial misregistration of the protons around the object) varies depending on screw orientation [see Eq. 1 and Fig. 3 in ref. (13) for a mathematical description]. We found a threefold reduction in susceptibility artifact size (Figs. 4 and 5) when the screw was parallel to B_0 versus perpendicular to it. Although it is not always possible to align a patient's implanted metallic hardware with B_0, in certain cases, one can choose an appropriate MR scanner for the patient. For example, an open MR system with B_0 passing from anterior to posterior would be preferred for patients with spinal pedicle screws, whereas a traditional magnet with B_0 passing from superior to inferior would be better for patients with hip prostheses.

Frequency Matrix, FOV, and Slice Thickness

Artifacts can be reduced by minimizing voxel volume in the frequency direction (2,6,11). By making the voxels smaller in the frequency direction, intravoxel phase dispersion is decreased, thereby reducing the artifact close to the object. We found that increasing the frequency matrix (Fig. 7A) and decreasing the slice thickness (Fig. 7B) moderately reduced susceptibility artifact size. De-

creasing the FOV had only a minimal effect (Fig. 7D). Voxel volume did not correlate well with artifact size (Fig. 6) and varied considerably depending on the selection of imaging parameters used to generate a given voxel volume. This differs from the results reported by Petersilge et al. (2), who found that artifact size was reduced by decreasing voxel volume. Unfortunately, their report did not explicitly describe the individual components used to calculate voxel volume; therefore, direct comparisons are not possible. The differences between the studies may also be due to different imaging techniques, as they performed only SE imaging.

Petersilge et al. (2) found that the most powerful indicator of artifact reduction using the SE technique was the FOV-to-frequency matrix ratio, which describes image resolution along the frequency axis. In our experiment using GRE imaging, we found the slice thickness-to-frequency matrix ratio to be a slightly stronger predictor of artifact reduction, followed by the FOV-to-frequency matrix ratio. However, in our data, these differences were small, and the main factor in both correlations probably resulted from the strong effects of increasing the frequency matrix parameter.

Phase Matrix

Artifacts are not affected by changing the phase matrix (2), as none of the three components of the susceptibility artifact is influenced by changes in the number of phase-encoding steps. Our data with the GRE technique also supported this finding (Fig. 7C).

Pixel Bandwidth

In theory, artifacts can be minimized by increasing the receiver bandwidth (Hz/pixel) (11,12). As the bandwidth/pixel increases, the effects from geometric distortion and intravoxel phase dispersion form a relatively smaller proportion of the total signal, thereby reducing image distortion. Although we did observe this phenomenon, the effect was minimal. This may be related to the fact that the receiver bandwidth setting on our MR scanner could be varied only from 10.4 to 15.6 kHz, a relatively small difference. Future experiments examining a larger bandwidth range may be helpful for further evaluation of the effects of this parameter on artifact size. On most MR systems, pixel bandwidth is not a separate parameter that can be varied; it is usually calculated by the MR scanner software from parameters such as the FOV, matrix size, and maximum gradient strength. As the signal-to-noise ratio is improved by using smaller bandwidths (less noise is sampled) and the effects on the susceptibility artifact are minimal, it is probably better to use smaller bandwidths to optimize image quality.

Strength of B_0

Artifacts can be minimized by using a magnet with a lower main magnetic field (4,9). The lower B_0 induces less magnetic field within a given substance, thereby reducing the local magnetic field distortion due to the inherent magnetic susceptibility of the substance. This points out a possible imaging benefit of using a low field MR system: namely, that the low magnetic field should be better suited to imaging patients with metallic implants. Perhaps a future study could be aimed at evaluating the benefits of susceptibility artifact reduction in relationship to the decreased signal-to-noise ratio obtained in such low field systems. We did not test this parameter in our study, as we did not have access to a low field magnet.

CONCLUSION

We varied many common imaging parameters in a GRE imaging sequence in an attempt to understand and thereby optimize them for the smallest possible susceptibility artifacts. The greatest reduction in artifact size came from using a short TE. Alignment with B_0 also yielded a large decrease in artifact size; whenever possible, implanted prostheses should be aligned with the main magnetic field to minimize artifact size. Increasing the frequency matrix and decreasing the slice thickness also contributed substantially to reducing the artifact size. Parameters with negligible effect on artifact size include bandwidth, phase encode matrix, and FOV. Radiologists can easily adjust such parameters in their GRE imaging protocols to improve image quality in patients with implanted metallic devices.

Acknowledgment: The authors thank Scott Reeder, M.D., Ph.D., for his assistance with the data analysis and discussion.

REFERENCES

1. Czervionke LF, Daniels DL, Wehrli FW, et al. Magnetic susceptibility artifacts in gradient-recalled echo MR imaging. *AJNR* 1988;9:1149–55.
2. Petersilge CA, Lewin JS, Duerk JL, et al. Optimizing imaging parameters for MR evaluation of the spine with titanium pedicle screws. *AJR* 1996;166:1213–8.
3. Eustace S, Goldberg R, Williamson D, et al. MR imaging of soft tissues adjacent to orthopaedic hardware: techniques to minimize susceptibility artefact. *Clin Radiol* 1997;52:589–94.
4. Farahani K, Sinha U, Sinha S, et al. Effect of field strength on susceptibility artifacts in magnetic resonance imaging. *Comput Med Imag Graph* 1990;14:409–13.
5. Laakman RW, Kaufman B, Han JS, et al. MR imaging in patients with metallic implants. *Radiology* 1985;157:711–4.
6. Young IR, Cox IJ, Bryant DJ, et al. The benefits of increasing spatial resolution as a means of reducing artifacts due to field inhomogeneities. *Magn Res Imag* 1988;6:585–90.
7. Christoffersson JO, Olsson LE, Sjoberg S. Nickel-doped agarose gel phantoms in MR imaging. *Acta Radiol* 1991;32:426–31.
8. Bakker CJ, Bhagwandien R, Moerland MA, et al. Simulation of susceptibility artifacts in 2D and 3D Fourier transform spin-echo

and gradient-echo magnetic resonance imaging. *Magn Res Imag* 1994;12:767–74.
9. Frahm C, Gehl HB, Melchert UH, et al. Visualization of magnetic resonance-compatible needles at 1.5 and 0.2 Tesla. *Cardiovasc Intervent Radiol* 1996;19:335–40.
10. Ladd ME, Erhart P, Debatin JF, et al. Biopsy needle susceptibility artifacts. *Magn Res Med* 1996;36:646–51.
11. Reichenbach JR, Venkatesan R, Yablonskiy DA, et al. Theory and application of static field inhomogeneity effects in gradient-echo imaging. *J Magn Res Imag* 1997;7:266–79.
12. Vinitski S, Mitchell DG, Einstein SG, et al. Conventional and fast spin-echo MR imaging: minimizing echo time. *J Magn Res Imag* 1993;3:501–7.
13. Reeder SB, Faranesh AZ, Boxerman JL, et al. In vivo measurement of T*2 and field inhomogeneity maps in the human heart at 1.5 T. *Magn Res Med* 1998;39:988–98.